

## Article

# Carbon Quantum Dots from Lemon Waste Enable Communication among Biodevices

Federico Cali <sup>1</sup>, Valentina Cantaro <sup>1</sup>, Luca Fichera <sup>1</sup>, Roberta Ruffino <sup>1</sup>, Giuseppe Trusso Sfrazzetto <sup>1</sup> , Giovanni Li-Destri <sup>1,2</sup>  and Nunzio Tuccitto <sup>1,2,\*</sup> 

<sup>1</sup> Department of Chemical Sciences, Università degli Studi di Catania, Viale A. Doria 6, 95125 Catania, Italy; federico.cali@phd.unict.it (F.C.); M15000139@studium.unict.it (V.C.); luca.fichera@phd.unict.it (L.F.); roberta.ruffino@phd.unict.it (R.R.); giuseppe.trusso@unict.it (G.T.S.); giolides@unict.it (G.L.-D.)

<sup>2</sup> Consorzio per lo Sviluppo dei Sistemi a Grande Interfase, CSGI, Viale A. Doria 6, 95125 Catania, Italy

\* Correspondence: nunzio.tuccitto@unict.it

**Abstract:** A bioinspired method of communication among biodevices based on fluorescent nanoparticles is herein presented. This approach does not use electromagnetic waves but rather the exchange of chemical systems—a method known as molecular communication. The example outlined was based on the fluorescence properties of carbon dots and follows a circular economy approach as the method involves preparation from the juice of lemon waste. The synthesis is herein presented, and the fluorescence properties and diffusion coefficient are evaluated. The application of carbon dots to molecular communication was studied from a theoretical point of view by numerically solving the differential equation that governs the phenomenon. The theoretical results were used to develop a prototype molecular communication platform that enables the communication of simple messages via aqueous fluids to a fluorescence-detecting biodevice receiver.

**Keywords:** carbon dots; fluorescence; diffusion coefficient; molecular communication



**Citation:** Cali, F.; Cantaro, V.; Fichera, L.; Ruffino, R.; Trusso Sfrazzetto, G.; Li-Destri, G.; Tuccitto, N. Carbon Quantum Dots from Lemon Waste Enable Communication among Biodevices. *Chemosensors* **2021**, *9*, 202. <https://doi.org/10.3390/chemosensors9080202>

Academic Editor: João Prior

Received: 28 June 2021

Accepted: 28 July 2021

Published: 30 July 2021

**Publisher's Note:** MDPI stays neutral with regard to jurisdictional claims in published maps and institutional affiliations.



**Copyright:** © 2021 by the authors. Licensee MDPI, Basel, Switzerland. This article is an open access article distributed under the terms and conditions of the Creative Commons Attribution (CC BY) license (<https://creativecommons.org/licenses/by/4.0/>).

## 1. Introduction

Molecular communication (MoCo), as a general concept, refers to all the biological processes in which information is exchanged by means of molecular messengers [1], such as mRNA, ions, etc., or the chemical communication methods used by plants and animals based on pheromones or terpenes [2–4]. Recently, this term has been used to describe bio-inspired artificial communication systems, in which information particles (messengers) encode and transfer information between a transmitter and a receiver [5]. The predominant target application for artificial MoCo is biomedicine and cybernetics, and biological systems are the ideal environment for using information particles to connect bio-implanted devices and create networks according to the internet of things (IoT) approach [6]. A MoCo system needs three principal components to work: a transmitter, a communication medium, and a receiver. The transmitter releases small amounts of particles that propagate in a communication medium that may be liquid or gaseous. Through the communication medium, the particles reach the receiver, which is responsible for detecting and decoding the information encoded in the latter [7]. An initial and simple differentiation between MoCo systems relates to the distance travelled by the messengers between the transmitter and the receiver; MoCo can take place both at the micro or nanometric scale and through long-range communication systems, just like in natural biological systems [8,9].

The type of environment in which the signal is propagated can also generate communication differences, particularly if the propagation occurs in an open or closed system.

Open environments, like open air or aqueous pools, can be exploited for the propagation of a chemical signal, whereas confined environments, such as pipes or capillaries, are used for spontaneous diffusion of molecules or flow-driven transportation [10,11]. For this work, a prototype platform was used in which messenger transport takes place in a

closed system, specifically: in a microfluidic communication channel. This prototype is schematised in Figure 1 in a way that divides the transmitter, the communication channel, and the receiver.

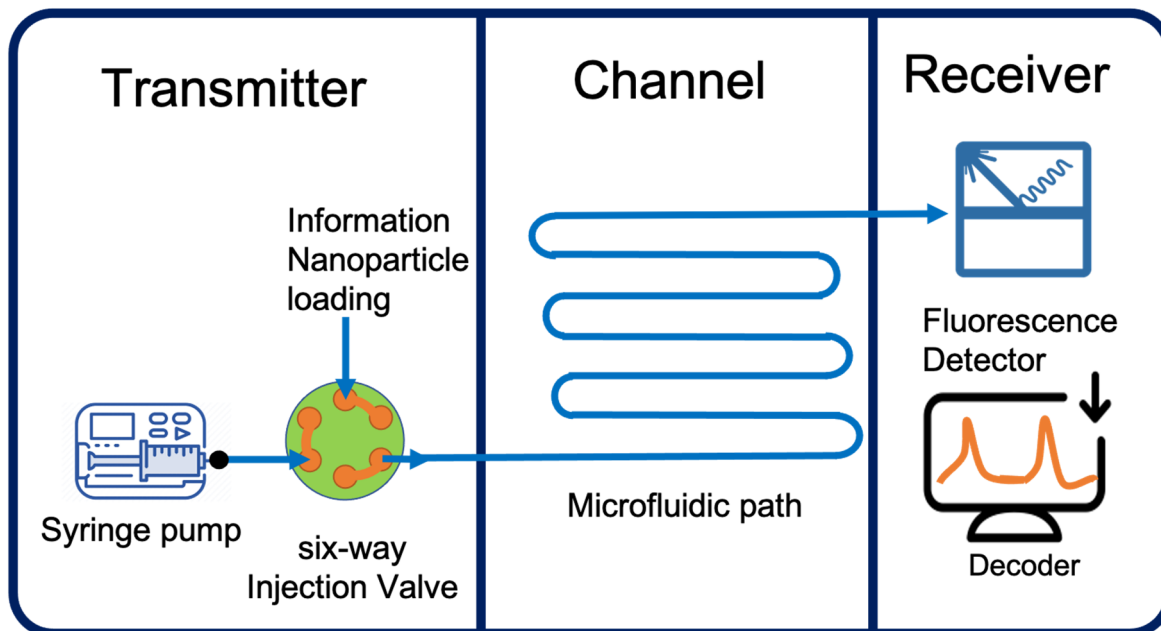


**Figure 1.** Schematic representation of the MoCo prototypal platform applied for communication through body fluid among implanted biodevices.

A system designed in this way is suitable for the creation of an artificial MoCo platform for the simple reasons that its transmitter enables generation of a chemical impulse that contains the information in its entirety, its communication channel enables the transport of the impulse, and its receiver picks up the signal and translates it into the initial message. In addition, such a system does not require much energy to generate and propagate signals, offering yet a further advantage.

Several signal modulation schemes have been suggested for use in MoCo and a further differentiation can be made based on the distinction between synchronised and non-synchronised communication. In the former, the concentration pulse of the messenger orders the encoding and decoding of messages. Upon application, the transmitter releases chemical messengers in an impulsive manner with each symbol bearing an associated and specific emission pattern. Of the numerous modulation schemes proposed in the literature, we selected the following: the on-off keying (OOK) and the concentration shift keying (CSK) [12–16]. With the binary scheme, in OOK modulation, the transmitter sends  $C_1$  chemical messengers for transmission of bit 1 but does not transmit a messenger when it codes bit 0. This means that the transmitter acts in apparent “on” and “off” states for the transmission of bits 1 and 0, respectively. In CSK, the transmitter releases chemical messengers  $C_1$  and  $C_0$  for the transmission of bits 1 and 0, respectively, with  $C_1$  representing the number of messengers higher than a specific threshold value and  $C_0$  the numbers lower. In this work, we exploited information nanoparticles (NPs) and used the OOK scheme in binary coding to send messages.

We have shown that the most suitable information NPs for these purposes are carbon nanoparticles (CNPs), more specifically, carbon dots (CDs) [17]. CDs, since their discovery in 2004, have aroused enormous interest not only for their optical properties but also for the simplicity with which they can be made biocompatible. CDs are generally produced whenever carbonization of a carbon source occurs. They are synthesized in the laboratory from carbon precursors of organic [18–21] or inorganic [22] nature mainly by pyrolysis or hydrothermal synthesis techniques. The simplicity with which CDs can be produced has

driven recent research into biomass as a carbon source. One of the first examples of using biomass to produce carbon quantum dots is based on simple single-step hydrothermal synthesis from orange juice [23]. We present here the use of lemon juice from waste lemons for the synthesis of high-value information NPs for biomedical applications in the emerging technological field of MoCo. The motivation behind the use of citrus fruit waste stems from its abundance: citrus is the most important fruit crop in terms of value worldwide. In 2016, the Food and Agriculture Organization of the United Nations FAO (2017) estimated the world's citrus fruit production at about 124.2 million tons, with oranges accounting for around 67 million tons. Globally, about 41 million tons of citrus fruits are industrially processed every year, mostly to produce juice [24]. However, the citrus fruit industry suffers considerably during the post-harvest phase from rot and thus reduced shelf life. Infection is by multiple fungal pathogens, including *Penicillium* species plures (spp.), *Phytophthora* spp., *Alternaria* spp., *Colletotrichum* spp., and *Geothrichum* spp., causing considerable losses [25,26]. The impact of these pathogens extends to the marketplace—the aesthetic quality of rot-affected fruit highly limits their sales potential. Thus, post-harvest rots have a large impact on the citrus fruit market: they reduce the shelf-life of fruit, are a limiting factor for their long-distance shipment, and impact storage and sales on vendor's shelves. The unfortunate result is huge quantities of unsold products, which is thus a large waste problem, causing significant economic losses.

Addressing this, we have the concepts of circular economics, green economics, zero-waste societies, and green chemistry—all underpinned by the valorisation of unsold products and waste. Indeed, the concept of circular economics incorporates new innovative fields of technology and, in many cases, the recovery of obsolete technology forms part of the development of new technologies. The same can be done for the development of nanotechnologies via the recovery of valuable precursors otherwise considered waste. Indeed, we present here the transformation of a low-value (virtually zero-value) waste into a high-value nanotechnology resource in the field of biomedicine. It was not the aim of this work to contribute to this innovation in the field of MoCo; however, importantly, we demonstrate the possibility of valorising a raw waste material (lemons) in line with the concept of circular economics by providing it a second use via preparation of highly fluorescent CDs for use in fields such as biomedicine.

## 2. Materials and Methods

CDs were synthesized from 100 mL of neat lemon juice (named lemon-only CDs) from the unsold waste of a large-scale retail shop (which the authors thank for the donation) or by adding this to 3.3 g of branched polyethylenimine (PEI) 50 wt.% in water (Aldrich) (named lemon-PEI CDs) in a 400 mL crystallizer. The crystallizer was then placed on a heating plate at 175 °C to trigger the decomposition process. When the colour of the solution changed from lemon yellow to caramel (typically after 15–20 min), three additions of 33 mL ultrapure water were made, 10 min apart. A fourth 33 mL aliquot of water was then added, and the resulting mixture was allowed to cool to room temperature. The purification process of the CDs thus obtained was carried out in three steps. Firstly, the non-polar residues were removed by extraction with 15 mL of chloroform (Aldrich), mixing the solution of CDs with pure chloroform (Aldrich) in a separating funnel. After vigorous agitation, the organic phase was separated from the aqueous phase by exploiting the immiscibility between the two phases. This process was repeated three times, always using renewed chloroform. A dialysis purification process was then carried out to remove the smaller but aqueously soluble residues. Dialysis was carried out by placing the CDs solution inside a dialysis tube (Membra-Cel MC18 with a molecular weight cut-off of 14,000 Dalton) and placing it in a 400 mL beaker filled with ultrapure water under constant agitation. In total, the water was replaced with fresh water three times (at 1-h intervals). A final dialysis run was also carried out overnight. Finally, a cryocentrifugation step was carried out for 1 h 50 min, at 6000 rpm, and 3 °C temperature. The supernatant was collected and used for subsequent characterization and MoCo experiments.

UV-vis analysis was performed using a Jasco V-750 spectrophotometer, and fluorescence analysis was performed using a Varian Cary Eclipse fluorescence spectrophotometer. The fluorescence yield was estimated with respect to sodium fluorescein dihydrate (Aldrich), which was used as a fluorescent standard. We considered an average diameter for both lemon-PEI CDs and lemon-only CDs, which were 1.5 nm and 1.8 nm, respectively with a density of 2.23 g/cm<sup>3</sup> (graphite density). Knowing these parameters, the weight of the individual nanoparticles was estimated. Next, we calculated the number of nanoparticles by knowing the weight of each one, and using Avogadro's number, we found the moles of CDs. From the latter, we estimated the molar mass. The resulting estimation was a molar mass for lemon-PEI NPs of approximately 2376 g/mol, and a molar mass for lemon-only CDs of approximately 4095 g/mol. The fluorescence yield percentage was calculated considering the maximum fluorescence intensity of both CDs and sodium fluorescein, normalized for molar concentration according to Equation (1).

$$\%_{\text{fluorescent yield}} = \frac{\frac{I_{\text{Max CDs}}}{M_{\text{CDs}}}}{\frac{I_{\text{Max STD}}}{M_{\text{STD}}}} \cdot 100 \quad (1)$$

where,  $I_{\text{Max STD}}$  is the maximum fluorescence intensity of the  $M_{\text{STD}}$  molar solution of sodium fluorescein, and  $I_{\text{Max CDs}}$  is the maximum fluorescence intensity of the  $M_{\text{CDs}}$  molar solution—estimated according to the previous CD procedure. The choice of the concentration of the NP suspensions was made considering the concentration-quenching effects of the CDs [27]; thus, the concentration chosen was based on the maximum fluorescence yield. Infrared analysis was obtained using a PerkinElmer spectrometer. To carry out the characterisation using the Fourier Transform Infrared (FT-IR) technique, we first dried a small amount of CDs. We then prepared a tablet consisting of 1% nanoparticles and the remaining part of anhydrous KBr. The FT-IR spectrum was acquired over an interval of 4000 to 500 cm<sup>-1</sup>, with a wavenumber step of 0.1 cm<sup>-1</sup>. Thirty-six subsequent scans were added. Atomic force microscopy (AFM) images were obtained using a Nanoscope IIIA multimode apparatus from Digital Instruments (Santa Barbara, CA, USA) used in tapping mode in air on a silicon substrate. Tap 300 G silicon probes from Budget Sensors, with a nominal resonance frequency of 300 kHz, were employed. NMR-DOSY information was gathered using a Varian UNITY Inova 500 MHz spectrometer (<sup>1</sup>H at 499.88 MHz, <sup>13</sup>C NMR at 125.7 MHz) equipped with a pulse field gradient module (Z axis) and a tuneable 5 mm Varian inverse detection probe (ID-PFG). Simulations of the transport process in MoCo were performed using Comsol Multiphysics software and its two interfaces “Laminar Flow” and “Transport of Diluted Species.” In the specific case, we modelled a tube 200 mm long and 0.40 mm wide; we used a flow velocity of 5.7 mm/s and a concentration of the transported substance of 10<sup>-3</sup> mol/m<sup>3</sup>. Two diffusion coefficients (D1 and D2) whose ratio was equal to 10 were used to obtain the simulations concerning the transport of the substance under lower and higher transverse diffusion conditions. A single diffusion coefficient of 1.5 × 10<sup>-10</sup> m<sup>2</sup>/s was used to perform the transmission of a simulated message. Further, to obtain the individual bits that make up the letters E, C, and O of the word “ECO,” the same simulation was repeated by sending the substance with a concentration of 10<sup>-3</sup> mol/m<sup>3</sup> to receive bit 1 and sending no substance (concentration 0 mol/m<sup>3</sup>) to receive bit 0. At the end of the iterative simulation, results were concatenated.

The MoCo platform was manufactured in-house. The transmitter was the Rheodyne 7725 6-way injection valve, which was used to inject 20 µL of particle solution into the flow. The channel consists of a Supelco teflon tube (ID 0.4 mm, OD 1.58 mm, length 200 mm, cat no 5-8702). The receiver was the fluorescence detector (Shimadzu RF535) connected to the pipe outlet. The control center consisted of a standard PC interfaced to a Keithley 2611 b used as a voltmeter. Python scripts were developed for data acquisition. The microfluidic system consisted of a piston pump controlled by a stepper motor to ensure constant flow speed and a Teflon tube that connected the transmitter and the receiver. The piston pump was designed in-house and made from components purchased at RS Components and

in-house printed parts made with a 3D printer (Alfawise u30 pro using PETG material). The detection of the fluorescence emitted by the nanomessengers was performed in flow by means of a detector from an in-flow fluorometer (from Shimadzu). An aqueous fluid with a viscosity of 3.5 mPa·s was used as a carrier.

### 3. Results

Two types of CDs were synthesised: one by using only lemon juice as a carbonaceous source (named lemon-only CDs) and the other by adding polyethyleneimine to the lemon juice (named lemon-PEI CDs). It is known that the synthesis of CDs in the presence of PEI has two positive effects on the quality of the CDs obtained [28,29]. Firstly, during the hydrothermal decomposition process, the PEI acts as an additional source of nitrogen, [30,31] although to a lesser degree than previously reported due to stability issues in the range up to 200 °C [32,33]. The result is an increase in the doping of the carbonaceous core of the CDs, improving the quantum yield [34,35]. Secondly, due to its polyimine structure, it acts as a passivating agent that functionalizes the surface of the CDs. The effect of surface passivation introduces emissive energy traps to promote recombination of electron–carbon pairs [36], resulting in a further increase in quantum yield.

The use of CDs as information NPs for MoCo requires not only unique optical properties but also adequate fluid dynamic properties to minimize information dispersal during transport. Therefore, investigation of CD dimensions is fundamental because dimensions correlate with fluid dynamic properties. In the specific case, a low size dispersion normalizes self-diffusivity effects thus minimizing chemical signal broadening during transport in the communication channel. It is known that the dispersion size of these NPs depends on the strategy of synthesis selected [37–39].

The AFM characterization reported in Figure 2a shows the typical distribution lemon-PEI CDs obtained with the adopted synthesis strategy. A section analysis was performed by observing the relative height of each NP in cross-sectional mode (example in Figure 2b). The histogram shows a size dispersion of about  $\pm 0.5$  nm, centered around 1.5 nm. This dimensional uniformity was obtained with a very simple and inexpensive synthesis strategy in terms of materials and solvents. Efficient synthesis derived from the combination of the use of PEI in the carbonization phase of the active components in lemon juice and from the dialysis process [40]. For lemon-only CDs, a size dispersion of about  $\pm 0.5$  nm was obtained, but this was time-centered around 2 nm (Figure 2c,d). However, slightly larger particles greater than 3 nm were also detected, which were probably formed due to the absence of PEI acting as a capping agent. For a complete characterization of the NPs, an extensive analysis of optical properties was performed using IR, UV–vis, and fluorescence spectroscopy. We found that lemon-only CDs displayed the typical properties of citric-acid-derived CDs that have been widely reported in the literature (not reported here) [41,42]. Regarding lemon-PEI CDs, the FT-IR spectra, reported in Figure 3a, shows the characteristic absorption peaks for the stretching vibration of C=O at  $1712\text{ cm}^{-1}$ , C–N or C–O bonds at  $1200\text{ cm}^{-1}$ , N–H and O–H at  $3370$  and  $3028\text{ cm}^{-1}$ , and C–H or O–H bending at  $1394\text{ cm}^{-1}$ . In addition, several characteristic peaks of PEI for lemon-PEI CDs, such as  $2940$  and  $2852\text{ cm}^{-1}$ , related to  $\text{CH}_2$  asymmetric and symmetric stretching vibration, and  $1566\text{ cm}^{-1}$  for a N–H bond, [43] could be seen. Considering the peaks of the bonds in which nitrogen is present, we could confirm N-doping and passivation with PEI. The UV–vis absorption spectrum (Figure 3b) indicated peaks at 350 and 230 nm. Specifically, the peak at deep UV is related to the  $\pi\text{--}\pi^*$  transition of aromatic systems in the carbonized core of the CNPs, whereas peaks at low energies around 300 nm are related to the  $n\text{--}\pi^*$  transition and surface functional groups, such as C=O [44,45].

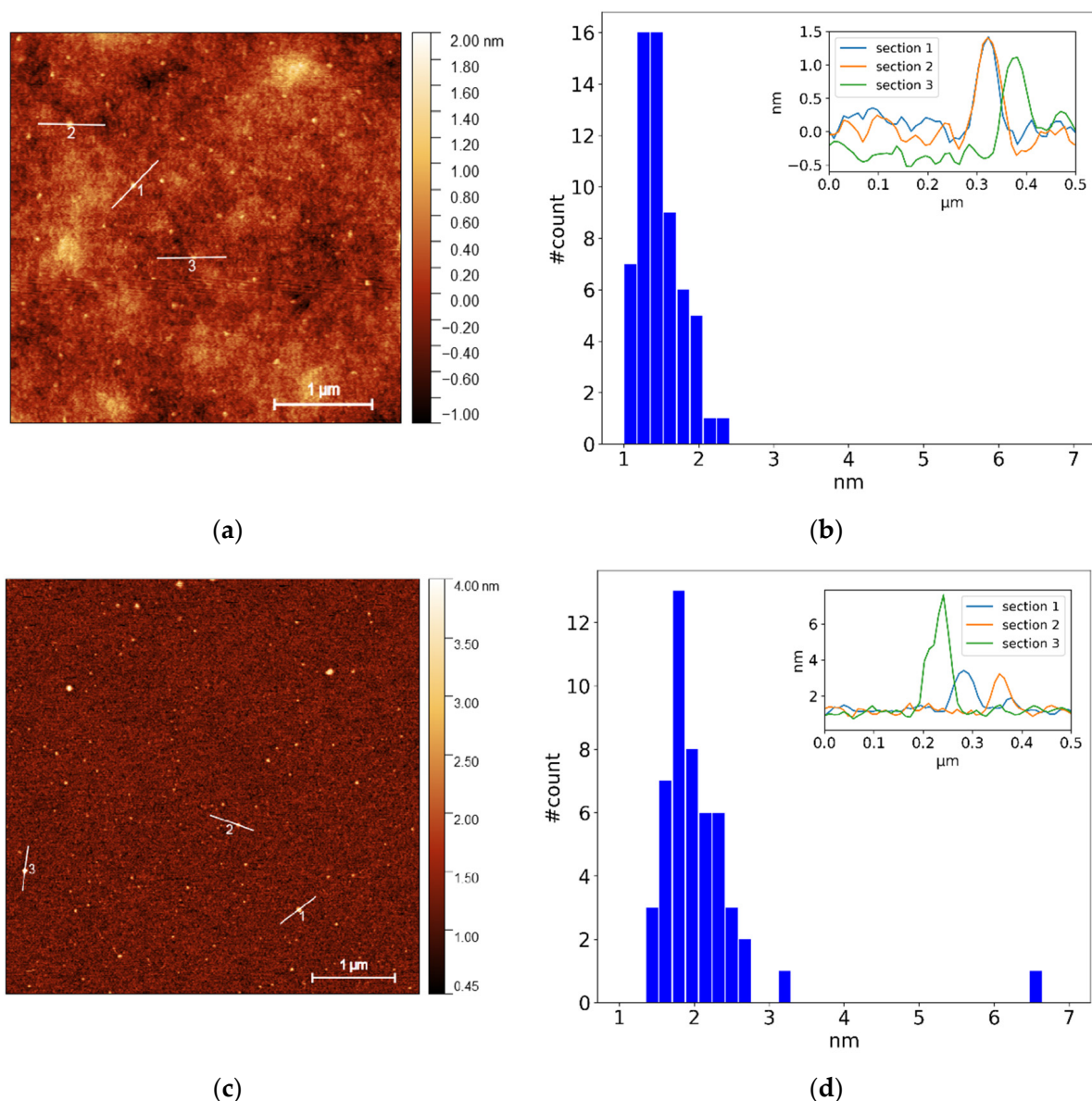


**Figure 2.** (a)  $5 \times 5 \mu\text{m}^2$  AFM image of lemon-PEI CDs deposited onto silicon substrate (z scale: 0–20°); (b) histogram analysis of lemon-PEI CDs' height obtained by several sections, three of which are represented in the inset; (c)  $5 \times 5 \mu\text{m}^2$  AFM image of lemon-only CDs deposited onto silicon substrate (z scale: 0–20°); (d) histogram analysis of height of lemon-only CDs obtained by several sections, three of which are represented in the inset.

In MoCo, a high fluorescence yield has a fundamental impact on the efficiency and reliability of information transmission. First, it allows for higher intensities at the receiver, thus improving the signal-to-noise ratio, reducing inter-symbol-interference effects. It enables use of lower concentrations of information NPs, therefore resulting in less consumption and, in the case of use in biological systems, less bio-impact. Figure 4a shows the photoluminescent (PL) spectra of the lemon-PEI CDs when irradiated with excitation wavelengths in the range of 250 to 400 nm. The strongest emission peak is centered at 470 nm upon excitation at 340 nm. The fluorescence map shown in Figure 4b appears as a small defined area in which the fluorescence falls within a relatively narrow window of emission wavelengths. This feature allows fluorescence to be easily distinguishable from any interferents present within the communication channel during application in MoCo. Lemon-only CDs show a broader fluorescence emission spectrum (Figure 4d) than PEI-treated CDs, although they are comparable in terms of intensity. The lemon-only CD

solution typically appears “cloudy” due to the presence of suspended particulate matter, as shown in Figure 4f, which cannot be separated by centrifugation (up to 15,000 rpm) or filtration (0.2  $\mu\text{m}$  of pore size).

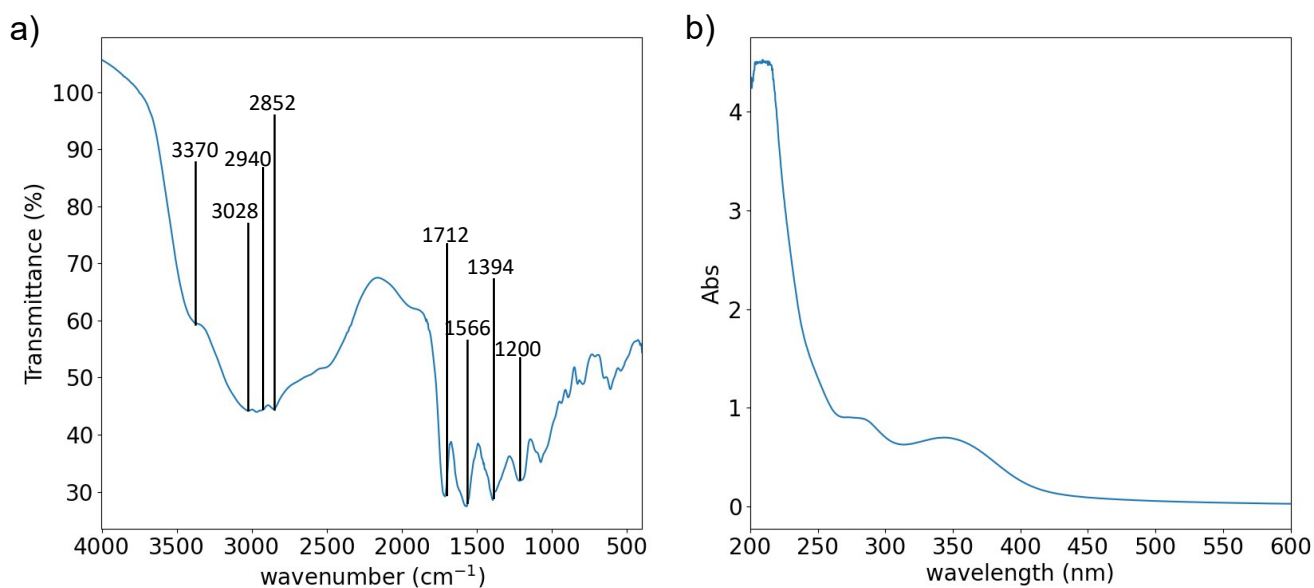


**Figure 3.** (a) FT-IR spectra and (b) UV-vis spectra of an aqueous suspension of lemon-PEI CDs.

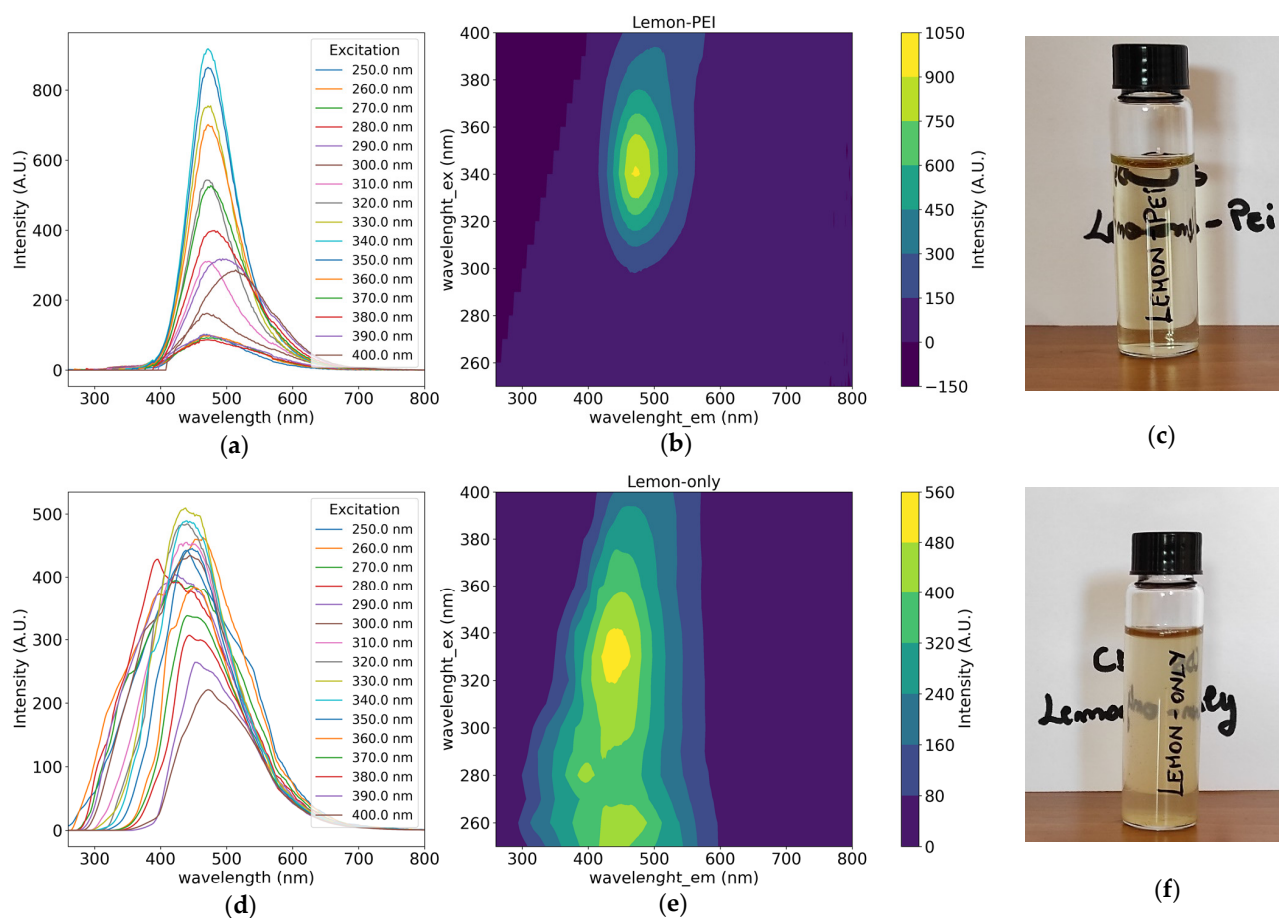


**Figure 4.** (a,d) Overlay of fluorescence spectra of aqueous suspensions of lemon-PEI CDs and lemon-only CDs, respectively, acquired at several excitation wavelengths as reported in the labels; (b,e) excitation–emission maps of aqueous suspensions of lemon-PEI CDs and lemon-only CDs, respectively; (c,f) photos depicting the qualitative appearance of the aqueous suspensions of lemon-PEI and lemon-only CDs.

Fluorescent NPs undergo self-quenching processes [46] that can be described by the Stern–Volmer mechanism and the following equation:

$$I(c_{det}) = k(1 - e^{-\varepsilon c_{det}d}) \cdot \frac{1}{1 + Kc_{det}} \quad (2)$$

where,  $\varepsilon$  is the molar extinction coefficient,  $d$  the optical path, and  $K$  the S–V constant [47]. For the lemon-PEI CDs, we started from a suspension with a concentration of 5.40 g/L and then carried out the various dilutions shown on the x-axis in Figure 5a. The trend of the fluorescence followed the expected curve according with Equation (2). Fluorescence increased with dilution because of the reduction in self-quenching up to reaching a maximum. After the strong dilution takes over, fluorescence decreases. The maximum fluorescence intensity was obtained for the suspension diluted 1:4, corresponding to a concentration of 1.35 g/L. The same procedure was carried out for the lemon-only CDs, this time starting from a concentration of 7.55 g/L and obtaining the maximum fluorescence intensity for the suspension diluted 1:6 (Figure 5b), corresponding to 1.26 g/L. Quantitatively, the fluorescence yield of lemon-PEI and lemon-only CDs was compared with sodium fluorescein, used as a standard, at the dilution showing the highest fluorescence (see Figure 5) [48]. We obtained no relevant difference between the fluorescence yields of lemon-PEI and lemon-only CDs, at 5.2% and 6.3%, respectively. Moreover, quenching effects were observed at concentrations that were much higher than those typically used in a MoCo experiment.

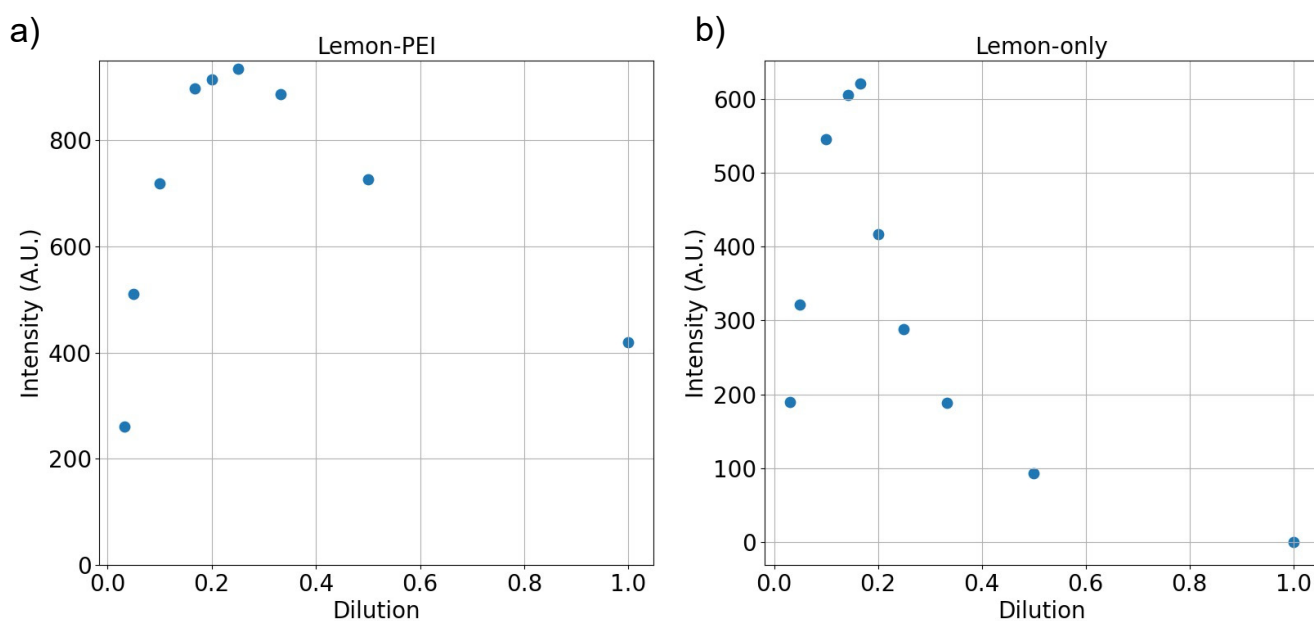


**Figure 5.** (a) Intensity of fluorescence peak as a function of the dilution of an aqueous suspension of lemon-PEI CDs ( $\lambda_{ex} = 340$  nm,  $\lambda_{em} = 470$  nm); (b) intensity of fluorescence peak as a function of the dilution of an aqueous suspension of lemon-only CDs ( $\lambda_{ex} = 330$  nm,  $\lambda_{em} = 440$  nm).

Another important feature for the application of CDs in MoCo relates to the physical properties that regulate diffusion and transport phenomena. A sizeable percentage of MoCo study is concerned with the propagation patterns of information particles within communication channels. The applicable models are highly variable and depend on the geometry of the channel, the channel environment, and the type of propagation involved, whether flow-assisted or purely diffusive [49–51]. The idea of applying MoCo to biological systems requires rigorous study of all possible contexts, which, as it stands, remain only partially theorized [52–54]. Above all, it is necessary to follow an experimental approach, which is currently not very common. From a theoretical point of view, we can start with

the models concerning the transport of matter within confined systems such as capillaries, where a continuous flow assists the movement of information particles. This study can be conducted by exploiting the advection–diffusion model (3):

$$\partial C/\partial t = \nabla \cdot (D \nabla C) - \nabla \cdot (\nu C) \quad (3)$$

where,  $C$  is the concentration of the bit of messengers released for communication in the body vessel,  $t$  is the time,  $D$  is the diffusion coefficient of the messenger, and  $\nu$  is the flow velocity of the body fluid. It must be considered that both the coefficient  $D$  and the velocity, from a numerical point of view, are tensors and depend strongly on the fluid dynamic conditions of the communication channel. With the aim of applying MoCo in biological environments, like in bloody vases, in a circular section capillary with a diameter of less than a millimetre and velocity in the order of mm/s, the flow can be considered laminar [55], and therefore the phenomena of dispersion of information particles during transport depends on the shape of the laminar flow profile and the diffusion coefficient, [56] whose contribution requires further investigation. Assuming the value of the diffusion coefficient is isotropic, it is possible to deconstruct it into two contributions: axial and transversal to the flow. The shape of the laminar flow makes the information particles moving along the capillary “arrow”-shaped. This is clearly visible in the simulation results reported in Figure 6b. The effect of the axial contribution on dispersion of the NPs is negligible with respect to the consequence of NPs’ transportation carried by the flow. Concerning the transversal diffusion, in the case of high-aspect-ratio channels (such as microfluidic channels in bloody vessels) the effect of this component is much more pronounced. NPs experience two concentration gradients driving the dispersion: (i) in the front from the centre towards the walls and (ii) in the tail from the walls towards the centre. This is schematized in Figure 6a. As time increases, and as the nanoparticle bit moves toward the detector, transverse scattering will minimize the arrow effect. This is schematized in Figure 6b and is clearly visible in the simulation results reported in Figure 6d.

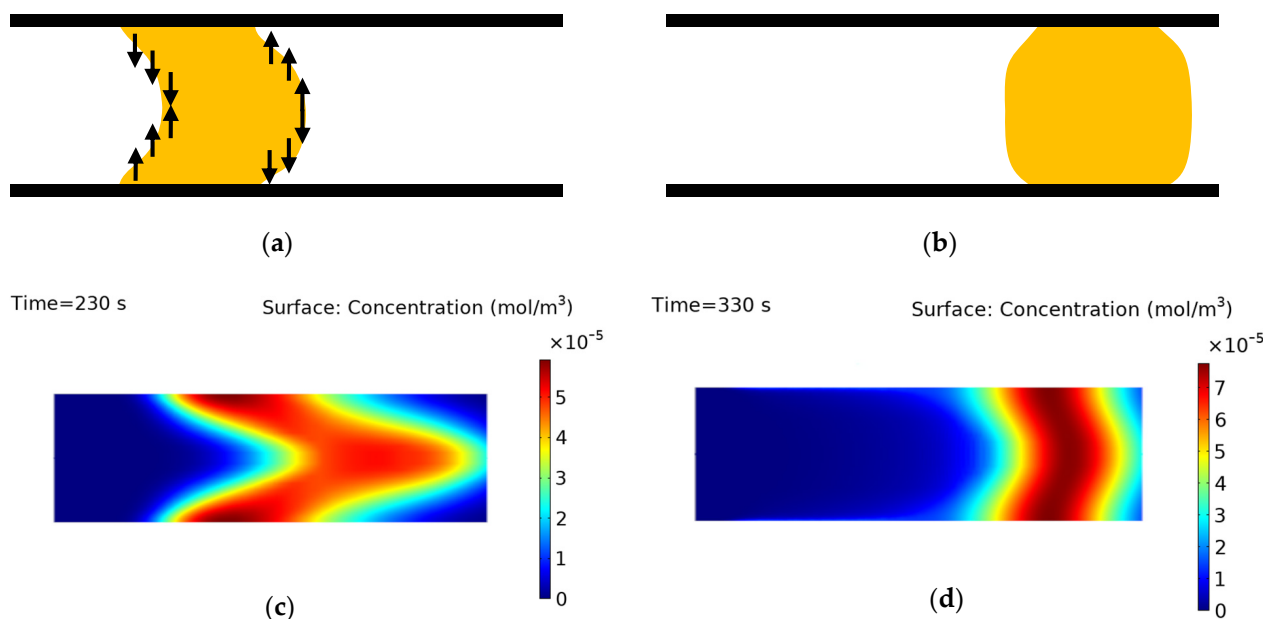


**Figure 6.** (a) Schematic representation of the transversal diffusion following concentration gradients; (b) schematic representation of the effect of the transversal diffusion at high diffusion coefficient; false colour map of simulated molecular messenger concentration distribution with lower diffusion coefficient (c), and with higher diffusion coefficient (d).

Thus, estimating the diffusion coefficient of CDs is essential to design and optimize the MoCo setup.  $D$  can be calculated using the Stokes–Einstein equation:

$$D = \frac{k_B T}{6\pi\eta r_n} \quad (4)$$

where,  $k_B$  is the Boltzmann constant,  $T$  is the temperature,  $\eta$  is the fluid viscosity, and  $r_n$  is the NP's radius, by considering CDs spherical objects. We estimated a diffusion coefficient of  $1.5 \times 10^{-10} \text{ m}^2/\text{s}$  by considering a temperature of 298.15 K, a viscosity of 1 mPa · s, and an average nanoparticle radius of 1.5 nm.

Experimentally, we measured the diffusion coefficient by the diffusion-ordered spectroscopy (DOSY) technique. The DOSY spectrum represented in Figure 7 was obtained using lemon-PEI CDs dispersed in deuterium oxide ( $\text{D}_2\text{O}$ ) at 27 °C. It indicates two different systems: the first relates to the CDs, described by a diffusion coefficient between  $1.5$  and  $2 \times 10^{-10} \text{ m}^2/\text{s}$ , and the second is connected to molecular residues probably derived from PEI and with a higher diffusion coefficient (about  $8 \times 10^{-10} \text{ m}^2/\text{s}$ ). We found a similar  $D$  in the case of only-lemon CDs.

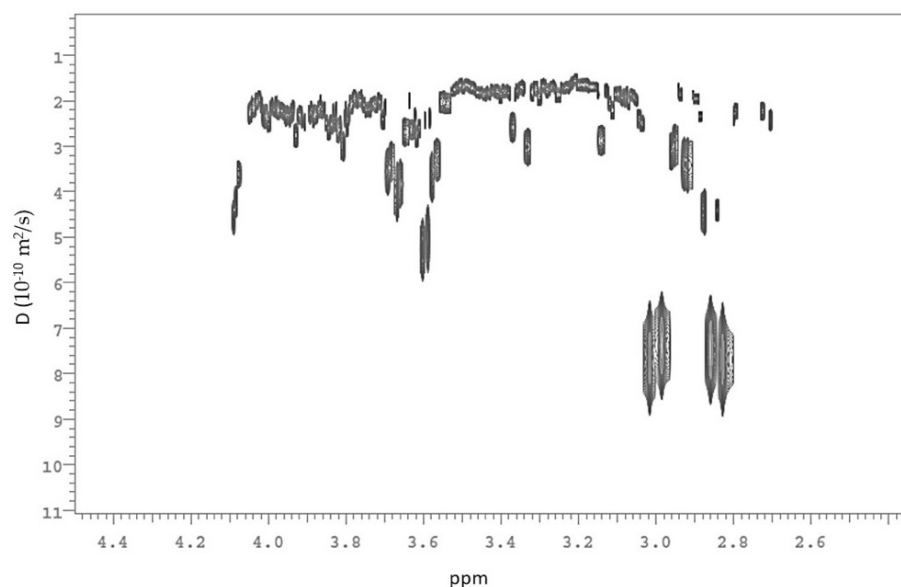


**Figure 7.** DOSY spectrum of lemon-PEI CDs dispersed in deuterium oxide ( $\text{D}_2\text{O}$ ). Diffusion coefficient values,  $D$ , are reported on the y-axis.

Holding the results of the complete synthesis and characterization of NPs, we designed, simulated, and experimentally validated a prototypal system for MoCo mimicking body fluid vessels using these CDs obtained from lemon waste as molecular messengers. Figure 8a shows the result of simulating a message sent by exploiting information NPs using an on-off-keying (OOK) modulation method [57] in binary coding. The message transmitted corresponds to the word “ECO” encoded in simplified ASCII. Figure 8b,c show the results for the actual experiment’s communication of the same message. Similar results were obtained with both types of CDs. The bit interval was 125 s. This value does not represent the condition of maximum efficiency. Further studies are needed to optimize this parameter. However, we can state that a perfect transmission of the message, in accordance with the simulation previously carried out, was achieved, enabling us to argue that being easily synthesized, eco-friendly, low cost, soluble/dispersible (in aqueous fluids), and easy to detect, the NPs prepared from lemon waste have the potential to be applied in emerging technological fields. Although the fluorescent nanoparticles were prepared from food waste sources, the results obtained can be considered comparable to what has already been reported in the literature with fluorescent nanoparticles synthesized from pure reagents. A

perfect transmission of the message, in accordance with the simulation previously carried out, was achieved, enabling us to argue that being easily synthesized, eco-friendly, low-cost, soluble/dispersible (in aqueous fluids), and easy to detect, the NPs prepared from lemon waste have the potential to be applied in emerging technological fields.

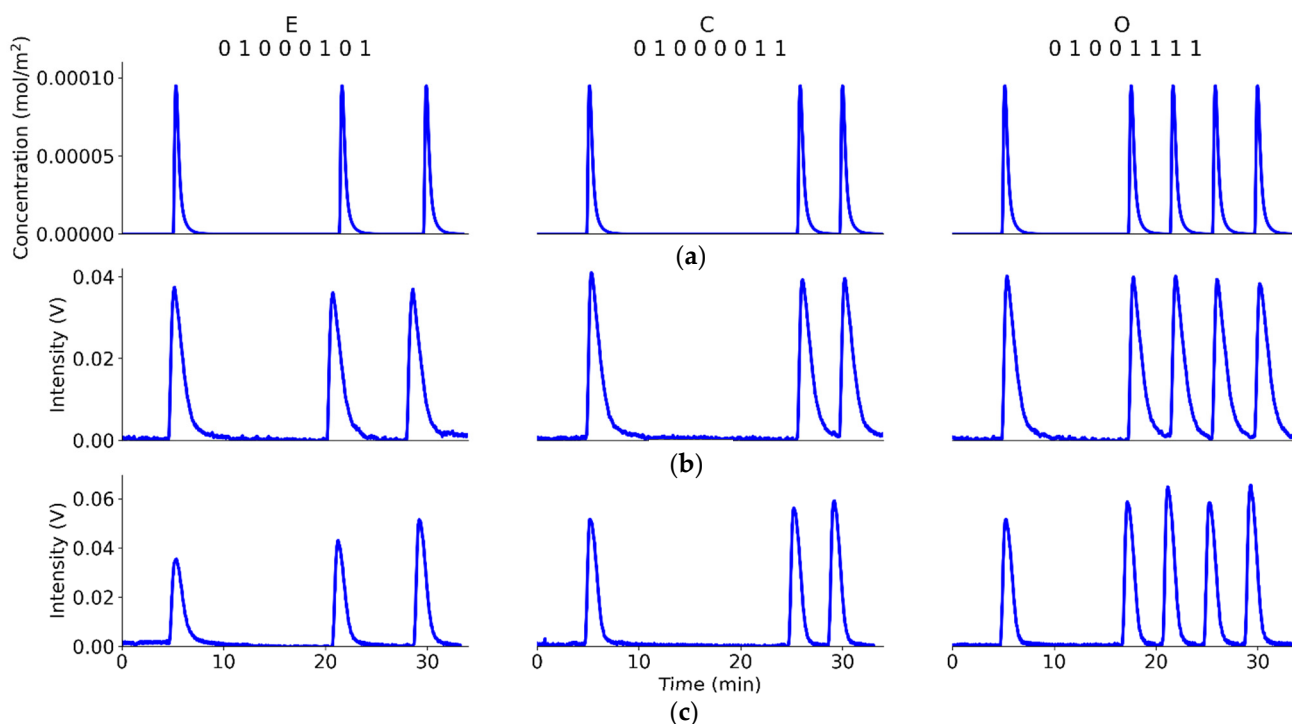


**Figure 8.** (a) Simulated message corresponding to “ECO” word in binary coding (simplified ASCII), obtained by modelling a capillary 0.40 mm in radius and 200 mm in length and setting the RMS velocity of the flow to 5.7 mm/s and the pulse of information particles to a volume of 20  $\mu$ L; experimentally, transmission of the word “ECO” was performed by using (b)lemon-only and (c) lemon-PEI carbon dots, respectively.

#### 4. Conclusions

MoCo is a new paradigm of bio-inspired communication where the transport of information occurs through information particles. Here, we showed that it is possible, when applied to MoCo, to turn a waste by-product from the citrus supply chain into information NPs, providing this waste with newfound added value. We showed a simple example of an application that can open the way to potential biomedical applications of CDs, which remains an unpredictable field of innovation. Although, at the moment, only the transmitted bit sequence was reported, and further studies are ongoing to mathematically characterize the pulse shapes with the aim of designing different detection schemes.

**Author Contributions:** Conceptualization, N.T.; methodology, V.C., L.F., F.C., R.R. and G.T.S.; software, L.F.; data curation, V.C., F.C., R.R. and G.T.S.; writing—original draft preparation, L.F., F.C. and V.C.; writing—review and editing, N.T. and G.L.-D.; visualization, F.C.; supervision, G.L.-D. and N.T.; project administration, N.T.; funding acquisition, N.T. All authors have read and agreed to the published version of the manuscript.

**Funding:** This research was funded by University of Catania, grant name “Programma ricerca di Ateneo UNICT 2020-22 linea 2 (NatI4Smart)”.

**Institutional Review Board Statement:** Not applicable.

**Informed Consent Statement:** Not applicable.

**Data Availability Statement:** Not applicable.

**Acknowledgments:** The authors thank Giovanni Marletta for his valuable advice, stimulating discussions, and mentoring. N.T. thanks the PRIMA project “Smart and innovative packaging, postharvest rot management and shipping of organic citrus fruit (BiOrangePack)”, a program supported by the European Union, for inspiring the author to develop nanomaterials from food waste.

**Conflicts of Interest:** The authors declare no conflict of interest.

## References

1. Farsad, N.; Eckford, A.W.; Hiyama, S.; Moritani, Y. On-Chip Molecular Communication: Analysis and Design. *IEEE Trans. Nanobioscience* **2012**, *11*, 304–314. [[CrossRef](#)] [[PubMed](#)]
2. Jackson, B.D.; Morgan, E.D. Insect chemical communication: Pheromones and exocrine glands of ants. *Chemoecology* **1993**, *4*, 125–144. [[CrossRef](#)]
3. Granström, K.M. Wood processing as a source of terpene emissions compared to natural sources. In *Air Pollution XV*; WIT Press: Southampton, UK, 2007; Volume I, pp. 263–272.
4. Darragh, K.; Orteu, A.; Black, D.; Byers, K.J.R.P.; Szczerbowski, D.; Warren, I.A.; Rastas, P.; Pinharanda, A.; Davey, J.W.; Garza, S.F.; et al. A novel terpene synthase controls differences in anti-aphrodisiac pheromone production between closely related *Heliconius* butterflies. *PLoS Biol.* **2021**, *19*, e3001022. [[CrossRef](#)] [[PubMed](#)]
5. Fichera, L.; Li-Destri, G.; Tuccitto, N. Nanoparticles as suitable messengers for molecular communication. *Nanoscale* **2020**, *12*, 22386–22397. [[CrossRef](#)]
6. Fichera, L.; Li-Destri, G.; Tuccitto, N. Fluorescent nanoparticle-based Internet of things. *Nanoscale* **2020**, *12*, 9817–9823. [[CrossRef](#)] [[PubMed](#)]
7. Moritani, Y.; Hiyama, S.; Suda, T. Molecular communication for health care applications. In Proceedings of the Fourth Annual IEEE International Conference on Pervasive Computing and Communications Workshops (PERCOMW'06), Pisa, Italy, 13–17 March 2006; p. 5553.
8. Unluturk, B.D.; Akyildiz, I.F. An End-to-End Model of Plant Pheromone Channel for Long Range Molecular Communication. *IEEE Trans. Nanobioscience* **2017**, *16*, 11–20. [[CrossRef](#)] [[PubMed](#)]
9. Meng, L.-S.; Yeh, P.-C.; Chen, K.-C.; Akyildiz, I.F. On Receiver Design for Diffusion-Based Molecular Communication. *IEEE Trans. Signal Process.* **2014**, *62*, 6032–6044. [[CrossRef](#)]
10. McGuinness, D.T.; Giannoukos, S.; Marshall, A.; Taylor, S. Experimental Results on the Open-Air Transmission of Macro-Molecular Communication Using Membrane Inlet Mass Spectrometry. *IEEE Commun. Lett.* **2018**, *22*, 2567–2570. [[CrossRef](#)]
11. Moore, M.J.; Nakano, T.; Enomoto, A.; Suda, T. Measuring Distance From Single Spike Feedback Signals in Molecular Communication. *IEEE Trans. Signal Process.* **2012**, *60*, 3576–3587. [[CrossRef](#)]
12. ShahMohammadian, H.; Messier, G.G.; Magierowski, S. Blind Synchronization in Diffusion-Based Molecular Communication Channels. *IEEE Commun. Lett.* **2013**, *17*, 2156–2159. [[CrossRef](#)]
13. Huang, Y.; Wen, M.; Yang, L.-L.; Chae, C.-B.; Ji, F. Spatial Modulation for Molecular Communication. *IEEE Trans. Nanobiosci.* **2019**, *18*, 381–395. [[CrossRef](#)] [[PubMed](#)]
14. Kuran, M.S.; Yilmaz, H.B.; Demirkol, I.; Farsad, N.; Goldsmith, A. A Survey on Modulation Techniques in Molecular Communication via Diffusion. *IEEE Commun. Surv. Tutorials* **2021**, *23*, 7–28. [[CrossRef](#)]
15. Qiu, S.; Guo, W.; Wang, S.; Farsad, N.; Eckford, A. A molecular communication link for monitoring in confined environments. In Proceedings of the 2014 IEEE International Conference on Communications Workshops (ICC), Sydney, NSW, Australia, 10–14 June 2014; pp. 718–723.
16. Akdeniz, B.C.; Pusane, A.E.; Tugcu, T. Optimal Reception Delay in Diffusion-Based Molecular Communication. *IEEE Commun. Lett.* **2018**, *22*, 57–60. [[CrossRef](#)]
17. Tuccitto, N.; Li-Destri, G.; Messina, G.M.L.; Marletta, G. Fluorescent Quantum Dots Make Feasible Long-Range Transmission of Molecular Bits. *J. Phys. Chem. Lett.* **2017**, *8*, 3861–3866. [[CrossRef](#)]
18. Thiyagarajan, S.K.; Raghupathy, S.; Palanivel, D.; Raji, K.; Ramamurthy, P. Fluorescent carbon nano dots from lignite: Unveiling the impeccable evidence for quantum confinement. *Phys. Chem. Chem. Phys.* **2016**, *18*, 12065–12073. [[CrossRef](#)]
19. Chatzimitakos, T.G.; Stalikas, C.D. Carbon nanodots from natural (re)resources: A new perspective on analytical chemistry. In *Handbook of Nanomaterials in Analytical Chemistry*; Elsevier: Amsterdam, The Netherlands, 2020; pp. 3–28.
20. Zhang, Z.; Sun, W.; Wu, P. Highly Photoluminescent Carbon Dots Derived from Egg White: Facile and Green Synthesis, Photoluminescence Properties, and Multiple Applications. *ACS Sustain. Chem. Eng.* **2015**, *3*, 1412–1418. [[CrossRef](#)]
21. Liang, Q.; Ma, W.; Shi, Y.; Li, Z.; Yang, X. Easy synthesis of highly fluorescent carbon quantum dots from gelatin and their luminescent properties and applications. *Carbon N. Y.* **2013**, *60*, 421–428. [[CrossRef](#)]
22. Liu, M.; Xu, Y.; Niu, F.; Gooding, J.J.; Liu, J. Carbon quantum dots directly generated from electrochemical oxidation of graphite electrodes in alkaline alcohols and the applications for specific ferric ion detection and cell imaging. *Analyst* **2016**, *141*, 2657–2664. [[CrossRef](#)]
23. Sahu, S.; Behera, B.; Maiti, T.K.; Mohapatra, S. Simple one-step synthesis of highly luminescent carbon dots from orange juice: Application as excellent bio-imaging agents. *Chem. Commun.* **2012**, *48*, 8835–8837. [[CrossRef](#)]
24. Food and Agriculture Organization of the United Nations (FAO). *Citrus: World Markets and Trade*; United States Department of Agriculture Foreign Agricultural Service: Washington, DC, USA, 2017; pp. 1–13.

25. Singh, V.; Deverall, B.J. *Bacillus subtilis* as a control agent against fungal pathogens of citrus fruit. *Trans. Br. Mycol. Soc.* **1984**, *83*, 487–490. [[CrossRef](#)]
26. Gerez, C.L.; Carbajo, M.S.; Rollán, G.; Leal, G.T.; de Valdez, G.F. Inhibition of Citrus Fungal Pathogens by Using Lactic Acid Bacteria. *J. Food Sci.* **2010**, *75*, M354–M359. [[CrossRef](#)] [[PubMed](#)]
27. Song, Y.; Zhu, S.; Xiang, S.; Zhao, X.; Zhang, J.; Zhang, H.; Fu, Y.; Yang, B. Investigation into the fluorescence quenching behaviors and applications of carbon dots. *Nanoscale* **2014**, *6*, 4676–4682. [[CrossRef](#)]
28. Yao, Y.; Niu, D.; Lee, C.H.; Li, Y.; Li, P. Aqueous Synthesis of Multi-Carbon Dot Cross-Linked Polyethyleneimine Particles with Enhanced Photoluminescent Properties. *Macromol. Rapid Commun.* **2019**, *40*, e1800869. [[CrossRef](#)] [[PubMed](#)]
29. Wang, C.; Xu, Z.; Zhang, C. Polyethyleneimine-Functionalized Fluorescent Carbon Dots: Water Stability, pH Sensing, and Cellular Imaging. *ChemNanoMat* **2015**, *1*, 122–127. [[CrossRef](#)]
30. Wu, X.; Wu, L.; Cao, X.; Li, Y.; Liu, A.; Liu, S. Nitrogen-doped carbon quantum dots for fluorescence detection of Cu<sup>2+</sup> and electrochemical monitoring of bisphenol A. *RSC Adv.* **2018**, *8*, 20000–20006. [[CrossRef](#)]
31. Park, Y.; Yoo, J.; Lim, B.; Kwon, W.; Rhee, S.-W. Improving the functionality of carbon nanodots: Doping and surface functionalization. *J. Mater. Chem. A* **2016**, *4*, 11582–11603. [[CrossRef](#)]
32. Zhu, X.; Liao, Q.; Liu, Q.; Wang, H.; Ding, Y.; Zeng, F. Synthesis of polyethylenimine-impregnated Al-fumarate metal-organic framework and its CO<sub>2</sub> adsorption characteristics. *Chin. Sci. Bull.* **2019**, *64*, 2441–2449. [[CrossRef](#)]
33. Quang, D.V.; Dindi, A.; Rayer, A.V.; Hadri, N.E.; Abdulkadir, A.; Abu-Zahra, M.R.M. Impregnation of Amines Onto Porous Precipitated Silica for CO<sub>2</sub> capture. *Energy Procedia* **2014**, *63*, 2122–2128. [[CrossRef](#)]
34. Manioudakis, J.; Victoria, F.; Thompson, C.A.; Brown, L.; Movsum, M.; Lucifero, R.; Naccache, R. Effects of nitrogen-doping on the photophysical properties of carbon dots. *J. Mater. Chem. C* **2019**, *7*, 853–862. [[CrossRef](#)]
35. Barman, M.K.; Jana, B.; Bhattacharyya, S.; Patra, A. Photophysical Properties of Doped Carbon Dots (N, P, and B) and Their Influence on Electron/Hole Transfer in Carbon Dots–Nickel (II) Phthalocyanine Conjugates. *J. Phys. Chem. C* **2014**, *118*, 20034–20041. [[CrossRef](#)]
36. Liu, C.; Zhang, P.; Zhai, X.; Tian, F.; Li, W.; Yang, J.; Liu, Y.; Wang, H.; Wang, W.; Liu, W. Nano-carrier for gene delivery and bioimaging based on carbon dots with PEI-passivation enhanced fluorescence. *Biomaterials* **2012**, *33*, 3604–3613. [[CrossRef](#)]
37. Yang, Y.; Kong, W.; Li, H.; Liu, J.; Yang, M.; Huang, H.; Liu, Y.; Wang, Z.; Wang, Z.; Sham, T.-K.; et al. Fluorescent N-Doped Carbon Dots as in Vitro and in Vivo Nanothermometer. *ACS Appl. Mater. Interfaces* **2015**, *7*, 27324–27330. [[CrossRef](#)] [[PubMed](#)]
38. Ma, X.; Li, S.; Hessel, V.; Lin, L.; Meskers, S.; Gallucci, F. Synthesis of N-doped carbon dots via a microplasma process. *Chem. Eng. Sci.* **2020**, *220*, 115648. [[CrossRef](#)]
39. Liu, X.; Liu, J.; Zheng, B.; Yan, L.; Dai, J.; Zhuang, Z.; Du, J.; Guo, Y.; Xiao, D. N-Doped carbon dots: Green and efficient synthesis on a large-scale and their application in fluorescent pH sensing. *New J. Chem.* **2017**, *41*, 10607–10612. [[CrossRef](#)]
40. Lu, S.; Guo, S.; Xu, P.; Li, X.; Zhao, Y.; Gu, W.; Xue, M. Hydrothermal synthesis of nitrogen-doped carbon dots with real-time live-cell imaging and blood–brain barrier penetration capabilities. *Int. J. Nanomed.* **2016**, *11*, 6325–6336. [[CrossRef](#)] [[PubMed](#)]
41. Stefanakis, D.; Philippidis, A.; Sygellou, L.; Filippidis, G.; Ghanotakis, D.; Anglos, D. Synthesis of fluorescent carbon dots by a microwave heating process: Structural characterization and cell imaging applications. *J. Nanoparticle Res.* **2014**, *16*, 2646. [[CrossRef](#)]
42. Zhang, W.; Shi, L.; Liu, Y.; Meng, X.; Xu, H.; Xu, Y.; Liu, B.; Fang, X.; Li, H.-B.; Ding, T. Supramolecular interactions via hydrogen bonding contributing to citric-acid derived carbon dots with high quantum yield and sensitive photoluminescence. *RSC Adv.* **2017**, *7*, 20345–20353. [[CrossRef](#)]
43. Li, L.; Liu, D.; Mao, H.; You, T. Multifunctional solid-state electrochemiluminescence sensing platform based on poly(ethylenimine) capped N-doped carbon dots as novel co-reactant. *Biosens. Bioelectron.* **2017**, *89*, 489–495. [[CrossRef](#)]
44. Dong, X.; Su, Y.; Geng, H.; Li, Z.; Yang, C.; Li, X.; Zhang, Y. Fast one-step synthesis of N-doped carbon dots by pyrolyzing ethanalamine. *J. Mater. Chem. C* **2014**, *2*, 7477–7481. [[CrossRef](#)]
45. Xu, M.; He, G.; Li, Z.; He, F.; Gao, F.; Su, Y.; Zhang, L.; Yang, Z.; Zhang, Y. A green heterogeneous synthesis of N-doped carbon dots and their photoluminescence applications in solid and aqueous states. *Nanoscale* **2014**, *6*, 10307–10315. [[CrossRef](#)]
46. Wang, W.; Damm, C.; Walter, J.; Nacken, T.J.; Peukert, W. Photobleaching and stabilization of carbon nanodots produced by solvothermal synthesis. *Phys. Chem. Chem. Phys.* **2016**, *18*, 466–475. [[CrossRef](#)]
47. Tuccitto, N.; Li-Destri, G.; Messina, G.M.L.; Marletta, G. Reactive messengers for digital molecular communication with variable transmitter–Receiver distance. *Phys. Chem. Chem. Phys.* **2018**, *20*, 30312–30320. [[CrossRef](#)]
48. Brannon, J.H.; Magde, D. Absolute quantum yield determination by thermal blooming. Fluorescein. *J. Phys. Chem.* **1978**, *82*, 705–709. [[CrossRef](#)]
49. Thakur, M.S.; Bhatia, V. Performance Analysis of Flow Assisted Diffusion Based Molecular Communication for D-MoSK. In Proceedings of the 2018 IEEE 87th Vehicular Technology Conference (VTC Spring), Porto, Portugal, 3–6 June 2018; pp. 1–6.
50. Pierobon, M.; Akyildiz, I.F. Noise Analysis in Ligand-Binding Reception for Molecular Communication in Nanonetworks. *IEEE Trans. Signal Process.* **2011**, *59*, 4168–4182. [[CrossRef](#)]
51. Kadloor, S.; Adve, R.S.; Eckford, A.W. Molecular Communication Using Brownian Motion with Drift. *IEEE Trans. Nanobioscience* **2012**, *11*, 89–99. [[CrossRef](#)]
52. Chude-Okonkwo, U.A.K.; Malekian, R.; Maharaj, B.T.; Vasilakos, A.V. Molecular Communication and Nanonetwork for Targeted Drug Delivery: A Survey. *IEEE Commun. Surv. Tutor.* **2017**, *19*, 3046–3096. [[CrossRef](#)]

53. Jamali, V.; Ahmadzadeh, A.; Wicke, W.; Noel, A.; Schober, R. Channel Modeling for Diffusive Molecular Communication—A Tutorial Review. *Proc. IEEE* **2019**, *107*, 1256–1301. [[CrossRef](#)]
54. Yang, K.; Bi, D.; Deng, Y.; Zhang, R.; Ur Rahman, M.M.; Ali, N.A.; Imran, M.A.; Jornet, J.M.; Abbasi, Q.H.; Alomainy, A. A comprehensive survey on hybrid communication for internet of nano-things in context of body-centric communications. *arXiv* **2019**, arXiv:1912.09424.
55. Berman, A.S. Laminar Flow in Channels with Porous Walls. *J. Appl. Phys.* **1953**, *24*, 1232–1235. [[CrossRef](#)]
56. Bicen, A.O.; Akyildiz, I.F. System-Theoretic Analysis and Least-Squares Design of Microfluidic Channels for Flow-Induced Molecular Communication. *IEEE Trans. Signal Process.* **2013**, *61*, 5000–5013. [[CrossRef](#)]
57. Arjmandi, H.; Ahmadzadeh, A.; Schober, R.; Kenari, M.N. Ion Channel Based Bio-Synthetic Modulator for Diffusive Molecular Communication. *IEEE Trans. Nanobioscience* **2016**, *15*, 418–432. [[CrossRef](#)] [[PubMed](#)]